

MECHANICAL PROPERTIES OF MULTI-YEAR SEA ICE  
TRIAXIAL TESTS STATUS REPORT

May 1984

by

G.F.N. Cox and J.A. Richter-Menge

U.S. Army Cold Regions Research and Engineering Laboratory  
Hanover, NH 03755

prepared for

Shell Development Company  
Minerals Management Service

MECHANICAL PROPERTIES OF MULTI-YEAR SEA ICE  
TRIAxIAL TESTS STATUS REPORT

May, 1984

Introduction

During the analysis of the Phase II triaxial test data it was found that the confined initial tangent modulus data of the ice were consistently lower than the initial tangent modulus data of the uniaxial or unconfined specimens. This caused some concern in that, intuitively, we would expect the confined modulus to be greater. Any confinement should reduce the axial displacement for a given load and thereby increase the measured modulus.

After checking our testing techniques and data reduction procedures, it was concluded that the lower confined modulus values were due to the use of the synthane end caps in the triaxial cell with externally mounted displacement transducers (Fig. 1). In effect, because sample displacements were measured outside the triaxial cell, the synthane end caps became a compliant element in an otherwise stiff loading system. If displacements were measured on the sample as in the uniaxial tests, the synthane end caps would not have presented any problems.

In addition to providing low confined modulus values, the synthane end caps and externally mounted displacement transducers also resulted in slightly lower ice strain-rates.

Despite the problems of using synthane end caps in the triaxial cell, it was hoped that the true ice modulus and strain-rate could be determined given the mechanical properties of the synthane. Uniaxial and triaxial tests were performed on a synthane specimen to determine the synthane

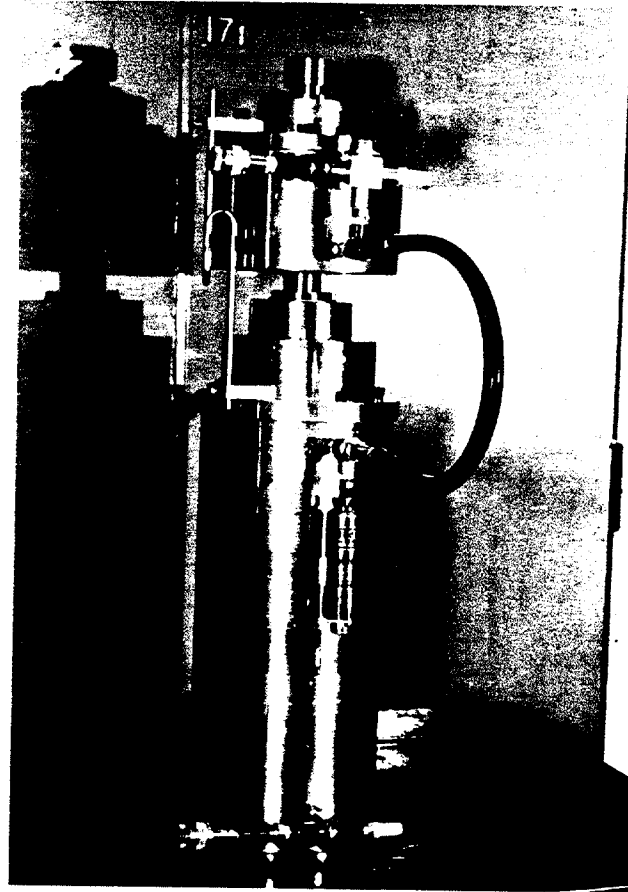


Figure 1: Triaxial cell with external mounts for extensometer.

properties and equations were derived to calculate the actual ice modulus and strain-rate from the test results. This status report presents our findings and recommendations for future triaxial testing.

#### Synthane Mechanical Properties

Uniaxial and triaxial compression tests were performed on a 4.2 in. dia., 14-in. long synthane sample at +20 and -10°C. The tests were conducted at two strain-rates,  $10^{-3}$  and  $10^{-5} \text{ s}^{-1}$ . Confining pressure - axial stress ratios of 0, 0.25, and 0.50 were used in the triaxial tests.

Based on our experience with the triaxial cell, means for measuring axial displacements on the triaxial cell were improved as shown in Figure 2. The test strain-rate in the new setup was controlled with the averaged output from two extensometers. The mounting positions of the extensometers were also moved from the upper cylinder to the shaft going into the triaxial cell. Previous test results indicated that the upper cylinder rotated slightly at the beginning of a test.

From the uniaxial and triaxial tests the synthane was found to have a modulus of  $7.77 \times 10^5 \text{ lbf/in.}^2$  and a Poisson's ratio of 0.21. The modulus and Poisson's ratio varied little with either strain-rate or temperature. The tests also provided a measure of the loading train deflection and cell elongation,  $1.4 \times 10^{-7} \text{ in./lbf}$ , which showed little variation with strain-rate, confining pressure, and temperature.

#### Correction for Synthane End Caps

Given the synthane properties and loading train deflection, it is possible to calculate the actual test strain-rate and ice modulus. The total measured displacement,  $\Delta \&_t$ , is equal to the sum of the displace-

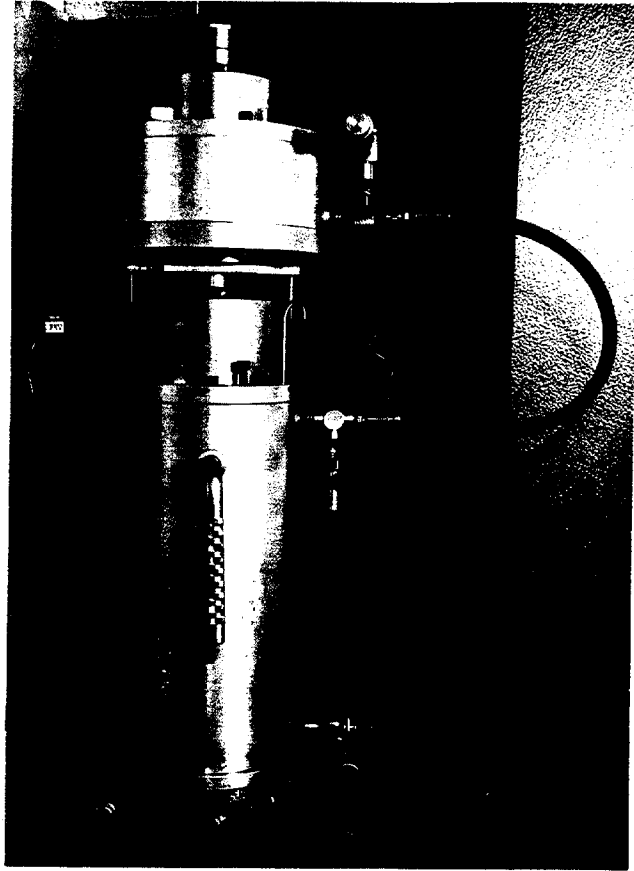


Figure 2: Triaxial cell with two external extensometers.

ments from the ice sample,  $\Delta l_s$ ; the synthane end caps,  $\Delta l_c$ ; and the loading train and cell walls,  $\Delta l_l$ :

$$\Delta l_t = \Delta l_s + \Delta l_c + \Delta l_l \quad (1)$$

or

$$\frac{\Delta l_t}{F} = \frac{\Delta l_s}{F} + \frac{\Delta l_c}{F} + \frac{\Delta l_l}{F} \quad (2)$$

where  $F$  is the applied load. From the synthane property tests, we have

$$\frac{\Delta l_l}{F} = C \quad (3)$$

where  $C = 1.40 \times 10^{-7}$  in./lbf and for the two end caps

$$\frac{\Delta l_c}{F} = \frac{2 l_c}{A_c E_c} (1 - 2 \nu_c k) \quad (4)$$

where

$l_c$  = end cap thickness (2 in.)

$A_c$  = end cap area (13.9 in.<sup>2</sup>)

$E_c$  = end cap modulus ( $7.77 \times 10^5$  lbf/in.<sup>2</sup>)

$\nu_c$  = end cap Poisson's ratio (0.21)

$k$  = confining pressure/axial stress ratio (0, 0.25, 0.50)

or

$$\frac{\Delta l_c}{F} = 3.72 \times 10^{-7} (1 - 0.42 k) \text{ in./lbf} \quad (5)$$

To put Equations (3) and (5) into perspective, a 10-in. long, 4-in. diameter ice sample with a modulus of  $7.5 \times 10^5$  lbf/in.<sup>2</sup> would deflect

$$\frac{\Delta l_s}{F} = 10.61 \times 10^{-7} (1-2 \nu_s k) \text{ in./lbf}$$

Under uniaxial or low confining pressure, deformation of the load train, cell walls, and end caps would account for about 33% of the total displacement.

By combining Equations (1), (3) and (4) and dividing by  $l_s$ , the sample length, we obtain

$$\frac{\Delta l_t}{l_s} = \frac{\Delta l_s}{l_s} + \frac{2 l_c F}{l_s A_c E_c} (1-2 \nu_c k) + \frac{CF}{l_s} \quad (6)$$

where  $\Delta l_t/l_s$  is the nominal strain,  $\epsilon_n$ , and  $\Delta l_s/l_s$  is the true sample strain,  $\epsilon_s$ . Solving for the true sample strain in terms of the nominal strain, we get

$$\epsilon_s = \epsilon_n - \frac{2 l_c F}{l_s A_c E_c} (1-2 \nu_c k) - C \frac{F}{l_s} \quad (7)$$

and by dividing by time,  $\Delta t$

$$\dot{\epsilon}_s = \dot{\epsilon}_n - \frac{2 l_c \dot{F}}{l_s A_c E_c} (1-2 \nu_c k) - C \frac{\dot{F}}{l_s} \quad (8)$$

From Equation (7) we can also obtain a relationship between the measured ( $E_m$ ) and actual ( $E_s$ ) confined ice modulus by multiplying by  $A_s/F$

where  $A_s$  is the cross-sectional area of the sample:

$$\frac{\epsilon_s A_s}{F} = \frac{\epsilon_n A_s}{F} - \frac{A_s}{l_s} \left( \frac{2 l_c}{A_c E_c} (1-2 \nu_c k) + C \right)$$

or

$$\frac{1}{E_s} = \frac{1}{E_m} - \frac{A_s}{l_s} \left( \frac{2 l_c}{A_c E_c} (1-2 \nu_c k) + C \right) \quad (9)$$

### Sample Calculations

The actual sample strain-rate during a test can be found from Equation (8) where by substitution we have

$$\dot{\epsilon}_s = \dot{\epsilon}_n - [3.72 \times 10^{-8}(1-0.42 k) + 1.4 \times 10^{-8}] \dot{F} \quad (10)$$

where  $\dot{F}$  is the load rate in lbf/s. At the beginning of the test  $\dot{F}$  is at its maximum and the actual strain-rate is at its lowest value for the entire test:

$$\dot{F} = \dot{F}_0 = A_s E_m \dot{\epsilon}_n$$

At the peak stress

$$\dot{F} = \dot{F}_p = 0$$

and

$$\dot{\epsilon}_s = \dot{\epsilon}_n$$

The average strain-rate up to the peak stress can be found by using

$$\dot{F}_{avg} = \frac{\sigma_m A_s}{t_m}$$

where  $\sigma_m$  is the peak stress and  $t_m$  is the time to failure.

The actual initial tangent modulus,  $E_s$ , can be directly determined from Equation (9). Equation (7) can be used to correct sample failure strains.

The mean measured modulus, mean strength, and mean time to failure for each of the six triaxial test conditions are given in Table 1. These values were used to calculate a representative initial strain-rate, average strain-rate and actual modulus for each test condition. The results are presented in Table 2.

Table 1: Mean modulus, strength, and time to failure values for each test condition.

$P/\sigma = 0.25$

	$\dot{\epsilon}_n = 10^{-5} \text{ s}^{-1}$	$\dot{\epsilon}_n = 10^{-3} \text{ s}^{-1}$
$T = -5^\circ\text{C}$	$E_m = 3.02 \times 10^5 \text{ lbf/in.}^2$ $\sigma_m = 415 \text{ lbf/in.}^2$ $t_m = 720 \text{ s}$	
$T = -20^\circ\text{C}$		$E_m = 4.71 \times 10^5 \text{ lbf/in.}^2$ $\sigma_m = 2141 \text{ lbf/in.}^2$ $t_m = 6.00 \text{ s}$

$P/\sigma = 0.50$

	$\dot{\epsilon}_n = 10^{-5} \text{ s}^{-1}$	$\dot{\epsilon}_n = 10^{-3} \text{ s}^{-1}$
$T = -5^\circ\text{C}$	$E_m = 2.87 \times 10^5 \text{ lbf/in.}^2$ $\sigma_m = 552 \text{ lbf/in.}^2$ $t_m = 1540 \text{ s}$	$E_m = 5.74 \times 10^5 \text{ lbf/in.}^2$ $\sigma_m = 1697 \text{ lbf/in.}^2$ $t_m = 4.97 \text{ s}$
$T = -20^\circ\text{C}$	$E_m = 3.56 \times 10^5 \text{ lbf/in.}^2$ $\sigma_m = 956 \text{ lbf/in.}^2$ $t_m = 1909 \text{ s}$	$E_m = 8.57 \times 10^5 \text{ lbf/in.}^2$ $\sigma_m = 3408 \text{ lbf/in.}^2$ $t_m = 7.24 \text{ s}$

Table 2: Corrected strain-rate and modulus for mean test data at each test condition

P/σ = 0.25

	$\dot{\epsilon}_n = 10^{-5} \text{ s}^{-1}$	$\dot{\epsilon}_n = 10^{-3} \text{ s}^{-1}$
T = -5°C	$\dot{\epsilon}_o = 8.21 \times 10^{-6} \text{ s}^{-1}$ $\dot{\epsilon}_{\text{avg}} = 9.66 \times 10^{-6} \text{ s}^{-1}$ $E_s = 3.68 \times 10^5 \text{ lbf/in.}^2$	
T = -20°C		$\dot{\epsilon}_o = 7.20 \times 10^{-4} \text{ s}^{-1}$ $\dot{\epsilon}_{\text{avg}} = 7.88 \times 10^{-4} \text{ s}^{-1}$ $E_s = 6.54 \times 10^5 \text{ lbf/in.}^2$

P/σ = 0.50

	$\dot{\epsilon}_n = 10^{-5} \text{ s}^{-1}$	$\dot{\epsilon}_n = 10^{-3} \text{ s}^{-1}$
T = -5°C	$\dot{\epsilon}_o = 8.44 \times 10^{-6} \text{ s}^{-1}$ $\dot{\epsilon}_{\text{avg}} = 9.80 \times 10^{-6} \text{ s}^{-1}$ $E_s = 3.40 \times 10^5 \text{ lbf/in.}^2$	$\dot{\epsilon}_o = 6.87 \times 10^{-4} \text{ s}^{-1}$ $\dot{\epsilon}_{\text{avg}} = 8.14 \times 10^{-4} \text{ s}^{-1}$ $E_s = 8.35 \times 10^5 \text{ lbf/in.}^2$
T = -20°C	$\dot{\epsilon}_o = 8.06 \times 10^{-6} \text{ s}^{-1}$ $\dot{\epsilon}_{\text{avg}} = 9.73 \times 10^{-6} \text{ s}^{-1}$ $E_s = 4.42 \times 10^5 \text{ lbf/in.}^2$	$\dot{\epsilon}_o = 5.33 \times 10^{-4} \text{ s}^{-1}$ $\dot{\epsilon}_{\text{avg}} = 7.43 \times 10^{-4} \text{ s}^{-1}$ $E_s = 1.61 \times 10^6 \text{ lbf/in.}^2$

Use of synthane end caps in the triaxial cell appears to have only a slight effect on the actual strain-rate during the test. The greatest difference between the nominal and actual strain-rate is found under test conditions where the ice is the stiffest, that is, at high pressure ( $k = 0.50$ ), high strain-rate ( $10^{-3} \text{ s}^{-1}$ ), and low temperature ( $-20^\circ\text{C}$ ). Even under these conditions, the actual and nominal strain-rates only differ by 25%.

The corrected modulus values still appear to be too low when they are compared to the modulus values obtained from the uniaxial test specimens. This suggests that there are other displacement errors not properly accounted for, such as closure across the end cap/loading piston interface. The attached Short Communication demonstrates that closure errors less than 0.002 in. can significantly reduce the initial tangent modulus at the beginning of the test when displacement transducers are not placed directly on the ice or the sample end caps.

#### Triaxial Cell Modification

In order to obtain accurate sample strains and ice moduli, we have enlarged the triaxial cell (Fig. 3) to accommodate an ice sample instrumented with a pair of linear variable differential transducers (LVDTs). The LVDTs are immersible and are capable of withstanding high hydraulic pressures. As we are interested in examining the post-yield behaviour of the ice and mechanical properties at large strains, the LVDTs are mounted on the sample end caps. Earlier work has shown that transducers mounted directly on the ice only provide reliable measurements up to the ice yield strength. The LVDTs are used to control the ice strain-rate and to measure sample strains and the initial tangent modulus.

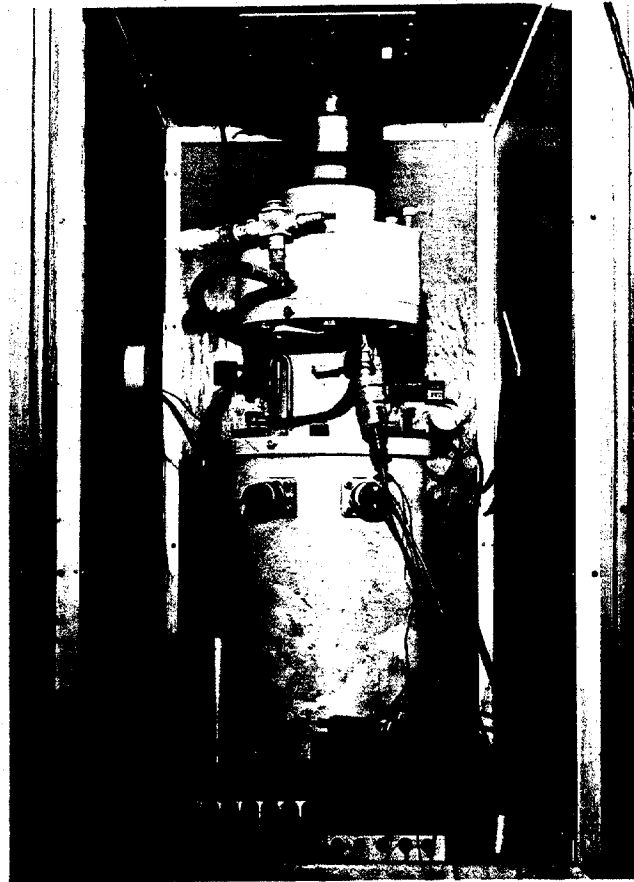


Figure 3. Modified triaxial cell.

A number of tests have been performed on our synthane test specimen and on first year, oriented sea ice to evaluate the new cell and LVDTs. The synthane test specimen was used to determine the deformation characteristics of the cell. Measurements of the cell's loading train deflection and the axial deformation of the cell wall were obtained for given loads and confining pressures. Unlike the previous triaxial cell, axial deformation of the cell wall is significant because of the larger annulus between the sample and cell wall. Tests were also performed on sea ice to compare external extensometer and internal LVDT measurements. We were interested in evaluating our formulas which are used to correct the Phase II extensometer readings for deformation of the end caps, loading train, and cell wall.

Stress-strain curves for two tests are shown in Figures 4 and 5. The test results in Figure 4 were obtained by controlling the sample strain-rate with the LVDTs mounted on the sample end caps. By measuring sample strains inside the cell on the sample, accurate strain-rates, strains, and moduli are obtained. The output from the external extensometers is also shown for comparison. The extensometers give a modulus that is too low and a failure strain that is too high. In Figure 5 the test results were obtained by controlling the strain-rate with the external extensometers as in the Phase II triaxial tests. Also shown is the actual stress-strain behavior experienced by the sample as measured by the LVDTs. Equations 7, 8 and 9 were used to correct the extensometer readings considering the deformation of the loading train, cell wall, and sample end caps. The corrected values are compared to the actual readings in Table 3. These results clearly demonstrate that the external extensometer measurements can

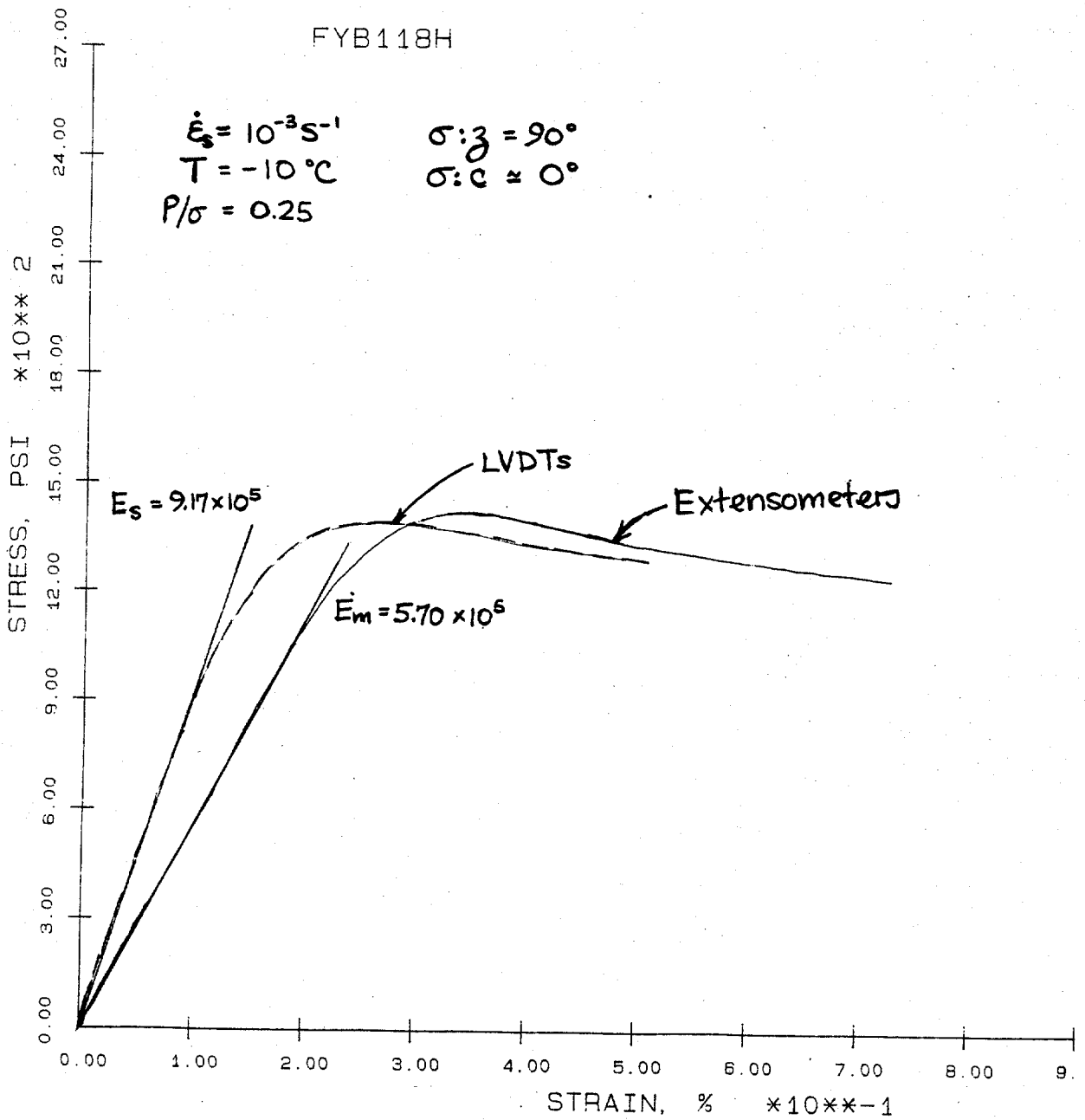


Figure 4. Stress-strain curves for sample whose strain-rate was controlled by LVDTs on the sample end caps inside the cell.

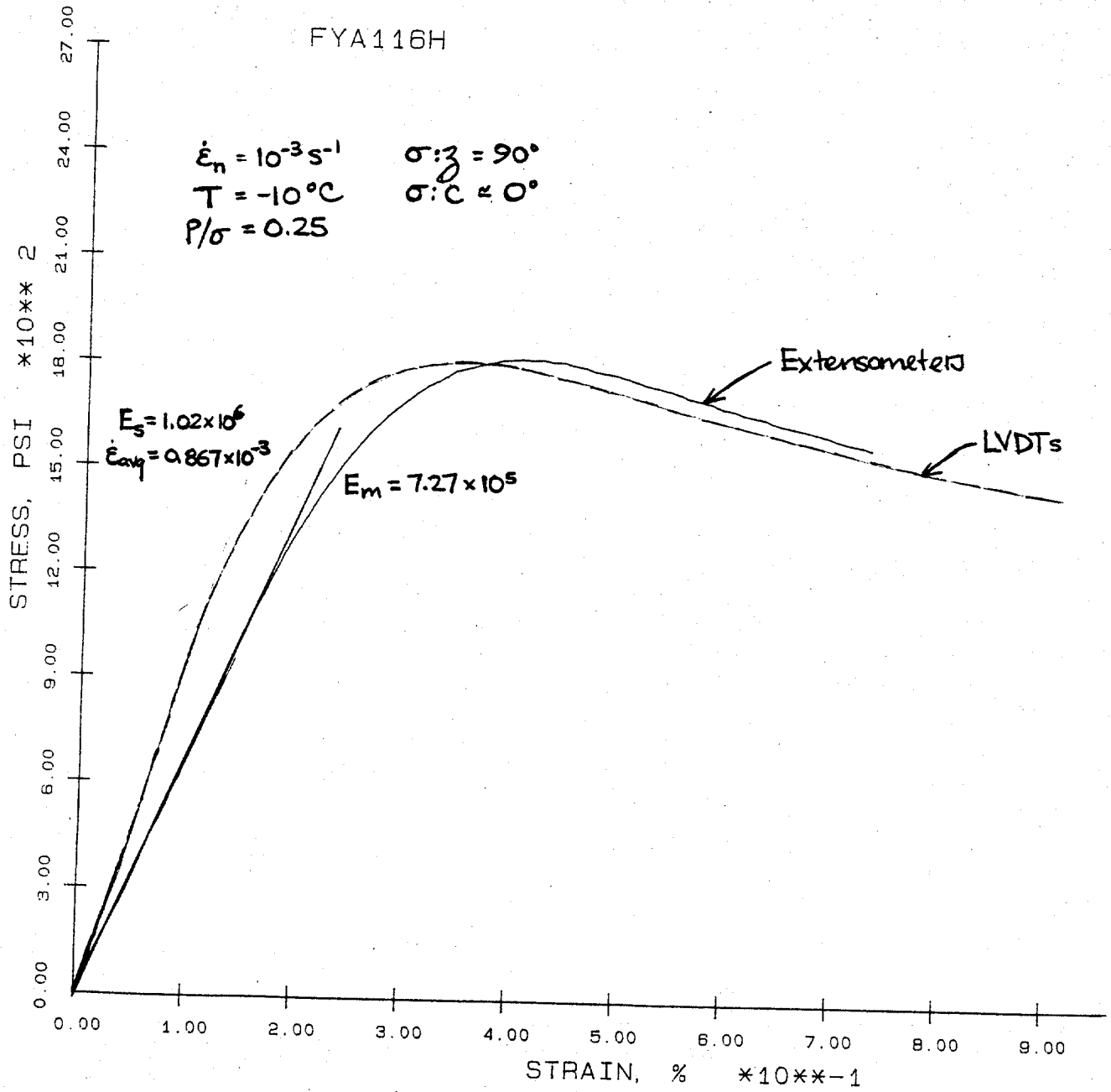


Figure 5. Stress-strain curves for sample whose strain-rate was controlled by external extensometers.

Table 3: Comparison between extensometer, corrected extensometer, and actual LVDT measurements for sample FYA116H.  $\epsilon_f$  is the sample failure strain.

	<u>Extensometers</u>	<u>Corrected Extensometers</u>	<u>Actual LVDTs</u>
$\dot{\epsilon}_0, s^{-1}$	$1 \times 10^{-3}$	$7.27 \times 10^{-4}$	$7.95 \times 10^{-4}$
$\dot{\epsilon}_{avg}, s^{-1}$	$1 \times 10^{-3}$	$8.63 \times 10^{-4}$	$8.67 \times 10^{-4}$
$\epsilon_f, \%$	0.413	0.362	0.363
$E, \text{ lbf/in.}^2$	$7.27 \times 10^5$	$9.14 \times 10^5$	$1.01 \times 10^6$

be corrected and used to calculate actual sample strains and strain-rates, provided that the cell deformation characteristics are known. However, due to some closure at the loading piston-end cap interface at the beginning of the test, the corrected initial tangent modulus value is still too low. Excellent agreement is obtained for the sample failure strain and average strain-rate because the sample displacement at yield is very large compared to the loading piston-end cap closure.

### Summary and Conclusions

Analyses of the Phase II triaxial modulus data indicated that our sample strains, as determined by an external extensometer, were in error. In addition to measuring the axial deformation of the sample, we were measuring the deformation of the synthane end caps, the loading train, and the cell wall. While these deformations were small, they resulted in low confined modulus values and slightly lower ice strain-rates.

Equations were then derived to correct the extensometer readings and evaluate the seriousness of the problem. Triaxial tests were also performed on a synthane test specimen to determine the mechanical properties of the synthane and deformation characteristics of the loading cell. The results indicated that actual ice strain-rates were up to 25% lower than the nominal strain-rate. The greatest difference between the actual and nominal strain-rate is found under test conditions where the ice is stiffest; that is, at high strain-rate, low temperature, and high confining pressure.

Corrected confined modulus data were still too low. It was determined that initial strain and modulus measurements were also affected by closure at the loading piston/end cap interface. Closures less than 0.002 in. were

sufficient to reduce measured moduli by 50%. While it was possible to correct the test data and determine the average strain-rate and failure strain for a given test, transducers in the cell were required to measure reliable modulus data.

The triaxial cell was enlarged and LVDTs mounted on the sample end caps were used to control the test strain-rate and measure sample strains. Additional testing proved that the equations developed to correct the Phase II strain and strain-rate data were valid and that transducers on the sample were only needed for accurate moduli data. Thus, only the confined modulus data from Phase II is lost. All the strength-strain-rate data is accurate, provided that corrections are made for deformation of the synthane end caps and cell.

SHORT COMMUNICATION

COLD REGIONS SCIENCE AND TECHNOLOGY

STATIC DETERMINATION OF YOUNG'S MODULUS IN SEA ICE

Jacqueline A. Richter-Menge  
Cold Regions Research and Engineering Laboratory  
Hanover, N.H. (USA)

Numerous tests are being performed at the Cold Regions Research and Engineering Laboratory in Hanover, New Hampshire, to determine the mechanical properties of arctic sea ice. By far the most difficult measurement to obtain accurately has been the initial tangent modulus, given by the force displacement curve and interpreted as Young's modulus. The purpose of this communication is to re-emphasize a warning by Mellor (1983) that a reliable initial tangent modulus cannot be determined unless axial strain measurements are made directly on the test specimen.

In unconfined uniaxial constant-strain-rate compression tests, we successfully determined the initial tangent modulus by mounting direct current displacement transducers (DCDTs) directly on the ice sample (Mellor et al., in press). Two DCDTs were located in the center portion of the sample, measuring the axial displacement over a gauge length of 5.5 inches (14 cm). The output of the transducers was averaged and recorded on an x-y plotter and strip chart. An extensometer was also used to measure full-sample axial displacements and to provide a control signal for the closed-loop testing system. This extensometer, mounted between the bonded

end caps of the sample, measured displacements over a length of 10 inches (25.4 cm). The ice-mounted DCDTs were not used to control the strain rate because each test was designed to measure force-displacement characteristics to 5% full sample strain. At these large strains the sample undergoes gross deformations, making the readings from the DCDTs unreliable. Measurements from both the DCDTs and the extensometer were reliable to  $\pm 0.5\%$  of the reading for axial displacements greater than 0.0001 in. ( $2.54 \times 10^{-3}$  mm). The axial strain measurements recorded by the DCDTs and the extensometer agreed very well up to peak load. The initial tangent modulus value was determined for each test using the initial slope of the force-displacement curve as recorded by the average of the DCDT measurements. Using the tangent modulus, we defined a Young's modulus which, on an average, agreed quite well with previous results (Cox et al., in press).

We were also interested in investigating the effect of confinement on the compressive behavior of sea ice. This included the influence that confinement might have on the initial tangent modulus. A conventional triaxial cell, pictured in Figure 1, was developed for maintaining a constant ratio between the applied axial stress and the confining pressure ( $\sigma_1 > \sigma_2, \sigma_3; \sigma_2 = \sigma_3; \sigma_2/\sigma_1 = \text{constant}$ ). On-ice axial displacement measurements were complicated by the fact that the ice sample was to be completely immersed in a high-pressure fluid. Considering the favorable agreement between the full sample (extensometer) and on-ice (DCDTs) axial displacement measurements in the uniaxial tests, we felt that a feasible alternative would be to measure the full-sample strain externally.



Figure 1: Triaxial cell

This alternative meant, however, that the recorded displacements would include ice end effects, end cap compression, and closure across an interface. The end cap compression was minimized by using aluminum end caps, which were very stiff relative to the ice. The interface of closure occurred between the loading piston and the top end cap of the sample. At this interface, we often had an imperfect contact due to a lack of parallelism in our machined samples. To correct for any lack of squareness, we measured the variation in sample height by running a comparator around the perimeter of the top end cap. Steel shimstock of the required gauge was then placed at the low point of the top end cap. Earlier evaluation of the uniaxial compression tests indicated that the use of shimstock was an effective means of compensating for the machining error.

It was still necessary to test the reliability of the external measurement more thoroughly. A series of three uniaxial compression tests was performed on ice samples at  $-10^{\circ}\text{C}$ . Two of the samples were tested at a constant strain rate of  $7.14 \times 10^{-6} \text{ s}^{-1}$ , and one was tested at a rate of  $7.14 \times 10^{-4} \text{ s}^{-1}$ . The ice samples were instrumented with DCDTs and an extensometer as described earlier. In addition, a pair of extensometers was mounted between the loading ram and the top end cap as shown in Figure 2. These extensometers were  $180^{\circ}$  apart, with one extensometer located at the low point of the upper end cap. Axial displacement measurements were recorded by the DCDTs mounted on the ice sample, the extensometer mounted between the bonded aluminum end caps, and the extensometers mounted across the shimmed interface. A comparison was then made of the initial portion

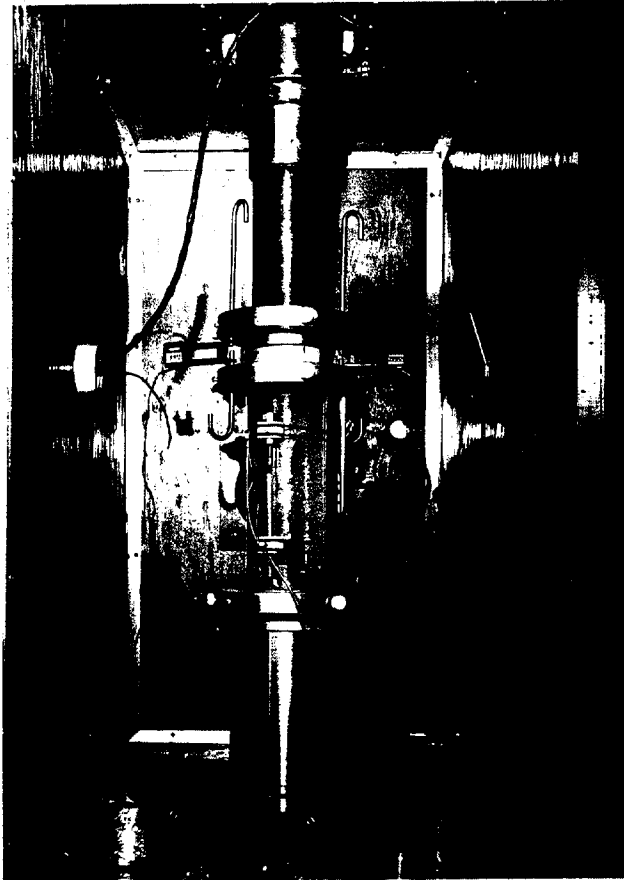


Figure 2: Test configuration to determine effect of closure.

of the force-displacement curves using 1) the DCDT output and 2) the full-sample extensometer output plus the displacement measurement across the shimmed interface. The latter curve simulated the axial displacements that would be obtained using the externally mounted extensometers on the triaxial cell.

The results are presented in Table 1, and Figure 3 shows a representative pair of curves. The initial tangent modulus values reported in Table 1 were defined by the initial slope of the recorded force-displacement curve.  $E_1(\text{GL})$  represents the modulus value determined using the axial displacement measured by the ice-mounted DCDTs, and  $E_1(\text{FS+P})$  is the modulus value determined using the full-sample and interfacial displacements. The percent reduction indicates the effect that external measurement techniques would have on the modulus value. The squareness value denotes the comparator readings on each sample and hence the shimstock used to correct for machining error. It is apparent that while the displacement across the shimmed interface is small, it is significant during the initial portion of the test, where displacements in the ice are also small. If we used the externally mounted extensometers in the triaxial tests, we could expect the initial tangent modulus value to be reduced to as much as one half the value that would be obtained in a uniaxial compression test on the same sample. As the axial force increases, the ice displacement continues to increase while the displacement across the shimmed interface remains constant. Therefore, the closure has a significant influence only during the initial portion of the test. Measurement of the displacement between

Table 1. Test results.

Sample No.	$E_i$ (GL) [GPa]	$E_i$ (FS+P)	Reduction [%]	Squareness [inches]
<u><math>\dot{\epsilon} = 10^{-5} \text{ s}^{-1}, T = -10^\circ\text{C}</math></u>				
12B	5.61	3.24	42	0.007
14C	5.14	4.26	17	0.009
<u><math>\dot{\epsilon} = 10^{-3} \text{ s}^{-1}, T = -10^\circ\text{C}</math></u>				
1C	7.19	4.53	37	0.003

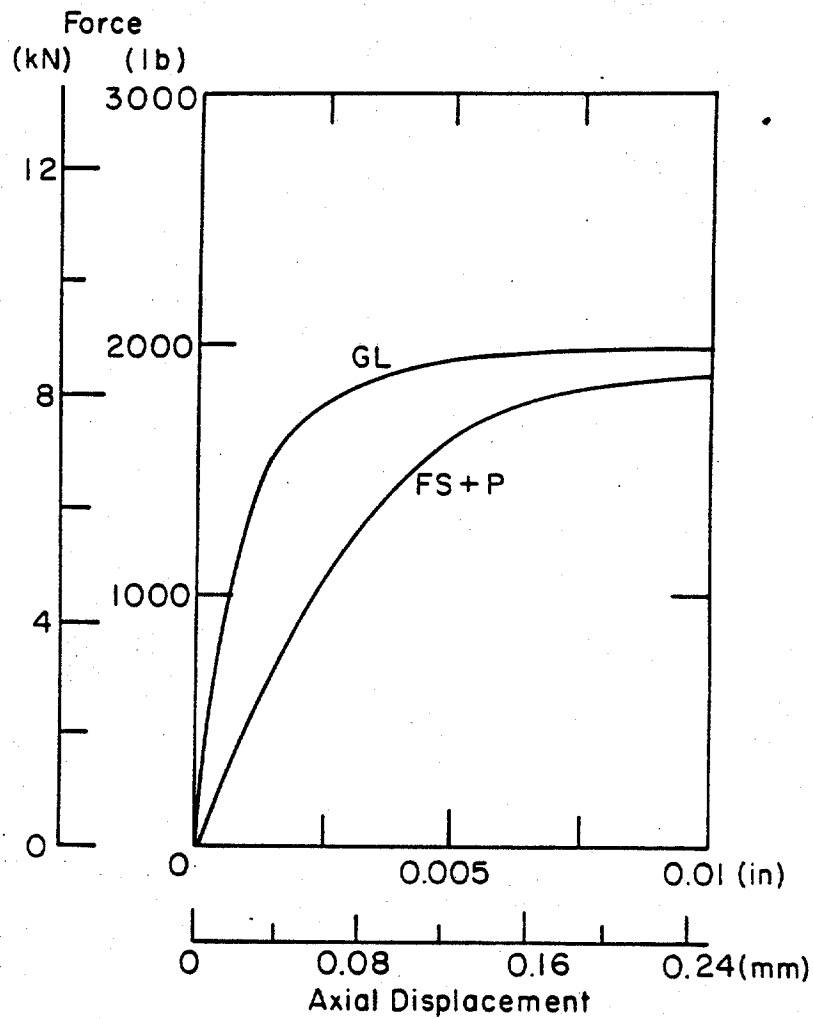


Figure 3a: Force-displacement curve for Sample 12B,  
 $T = -10^{\circ}\text{C}$ ,  $\dot{\epsilon} = 7.14 \times 10^{-6} \text{ s}^{-1}$ .

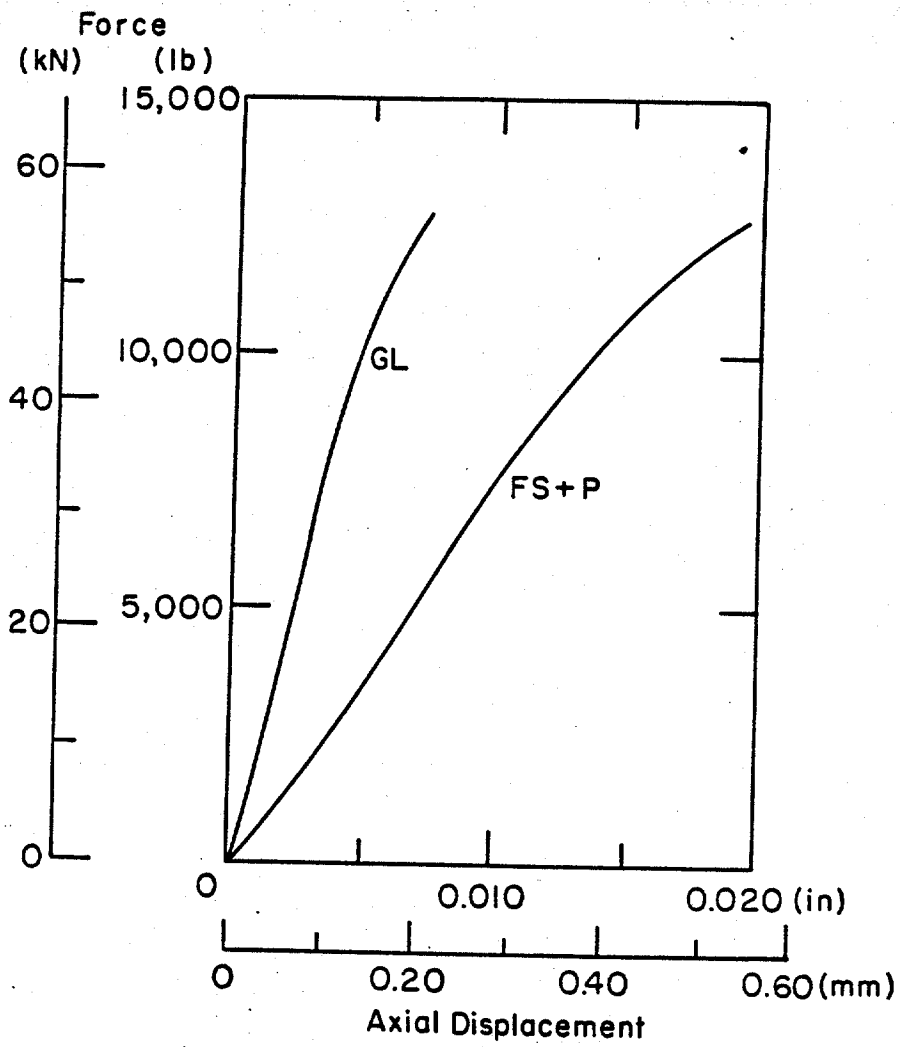


Figure 3b: Force-displacement curve for Sample 1C,  
 $T = -10^{\circ}\text{C}$ ,  $\dot{\epsilon} = 7.14 \times 10^{-4} \text{ s}^{-1}$ .

the loading ram and the top end cap indicates that the shimstock reduces the net closure at this interface to less than 0.002 inches.

These tests do indicate that displacement measurements made on the ice itself are necessary for reliably determining the initial tangent modulus, and hence Young's modulus. As a result of this study, modifications will be made to our triaxial cell so that it can accommodate an instrumented sample. Displacement transducers that can withstand high pressures, low temperatures and immersion will be used to measure the axial strain. These transducers will be mounted on the ice and the electrical signals that they transmit will pass through bulkhead connectors located in the cell wall. Once these changes have been completed, tests will be performed on ice samples to demonstrate the reliability of the displacement measurements.

#### ACKNOWLEDGEMENTS

The author is grateful to Mr. David Cole, Dr. Gordon Cox and Mr. Glenn Durell for many helpful suggestions. This work was supported by the U.S. Army Cold Regions Research and Engineering Laboratory, In-House Laboratory Independent Research (ILIR) DA Project 4A161101A91D, Work Unit 412, Triaxial Testing of Sea Ice.

## REFERENCES

- Cox, G.F.N., J.A. Richter, W.F. Weeks, M. Mellor and H.W. Bosworth (In press) Mechanical properties of multi-year sea ice, Phase I: Test results. U.S. Army Cold Regions Research and Engineering Laboratory, CRREL Report.
- Mellor, M. (1983) Mechanical behavior of sea ice. U.S. Army Cold Regions Research and Engineering Laboratory, Monograph 83-1.
- Mellor, M., G.F.N. Cox and H.W. Bosworth (In press) Mechanical properties of multi-year sea ice: Testing techniques. U.S. Army Cold Regions Research and Engineering Laboratory, CRREL Report.